[CANCER RESEARCH 64, 2656–2662, April 15, 2004]

Advances in Brief

Specific Histone Patterns and Acetylase/Deacetylase Activity at the Breakpoint-Cluster Region of the Human *MLL* Gene

Andriy Khobta,[1] Carmelo Carlo-Stella,[2] and Giovanni Capranico[1]

[1]G. Moruzzi Department of Biochemistry, Alma Mater Studiorum University of Bologna, Bologna, Italy, and [2]Medical Oncology Unit, Istituto Nazionale Tumori, University of Milan, Milan, Italy

Abstract

The *MLL* gene breakpoint-cluster region (BCR) is a known hot-spot for chromosomal translocations in human leukemias. We mapped core histone modifications and histone H1 along the *MLL* gene in Jurkat cells and human CD34$^+$ progenitor blood cells by chromatin immunoprecipitation. Within the BCR, we found specific histone patterns that were different from other genomic regions and a histone H1-free fragment at the telomeric end. Core histone acetylase/deacetylase activities were also found within the BCR. In the studied cell models, chromatin components at the *MLL* BCR suggest an asymmetric organization that may influence early molecular events eventually leading to chromosomal translocations.

Introduction

Translocations of the human *MLL* gene (chromosome 11 band q23) are detected in approximately 15% of patients with acute leukemias (1). Depending on the drug dose, up to 15% of patients treated with DNA topoisomerase II (top2) poisons and/or alkylating agents develop therapy-related leukemias characterized by chromosomal translocations at the *MLL* locus (1–3). Anticancer agents can generate double-stranded DNA breakage that, upon illegitimate DNA repair, may cause chromosomal translocations leading to fused genes coding for oncogenic products. Moreover, 60–80% of acute leukemias in infants under 12 months of age show *MLL* rearrangements suggesting that similar events might occur *in utero* leading to cell transformation (4).

Many translocations of the *MLL* gene map to a 8.3-kb *BamH*1 restriction fragment that spans exons 5–11 (5) and is known as breakpoint cluster region (BCR; Ref. 1). Thirty-seven different gene partners of *MLL* translocations have been identified in leukemic patients, and oncogenic products often retain a 5′ portion of the *MLL* gene[3] (1, 6). Interestingly, a major part of *MLL* translocations in *de novo* patients fall to a centromeric half of BCR, whereas translocations cluster to a telomeric portion in therapy-related leukemias (Refs. 1 and 6; Fig. 1). Several findings have provided evidence of the involvement of top2 or apoptotic nucleases in the generation of DNA cleavage that eventually leads to gene rearrangements (4, 6–9). However, several aspects of enzymes and DNA can influence DNA cleavage levels in living cells. It is well known that top2-mediated DNA breakage can markedly be altered in chromatin with respect to naked DNA substrates (10–12). Chromatin structure is a main factor that affects DNA accessibility to enzymes, including top2 and nucleases, and it can thus affect markedly the site and levels of enzyme-dependent DNA breaks at genomic regions in living cells. Nevertheless, chromatin organization remains to be fully defined along the human *MLL* gene and at the BCR.

The highly basic NH_2-terminal histone tails project away from nucleosomes and play a key role in higher-order chromatin structures and in interactions with other chromatin-associated regulatory proteins (13, 14). Post-transcriptional modifications of histones, such as acetylation, may favor the dissociation of DNA from histones allowing the interactions with transcription factors. On the other hand, histone modifications may represent a "histone code" that may determine the sequence and the nature of protein interactions that facilitate DNA transactions (15, 16). Acetylation of histones H3 and H4 occurs at specific lysine residues and has been associated with increased sensitivity to nucleases (17), which is generally considered a hallmark of an accessible conformation of chromatin, whereas decreased acetylation is often associated with repressed chromatin. Hyperacetylation of histones H3 and H4 is well documented in promoters of expressed genes and has been involved in the long-range regulation of chromatin structure (16, 18). Histone H1 can be present at higher levels in higher-order structures such as 30-nm fibers and is involved in the formation of repressed chromatin (19).

Therefore, we have mapped histone H3 and H4 acetylation and histone H1 along the *MLL* gene and at the BCR by chromatin immunoprecipitation in human cells to define specific molecular components of chromatin at the *MLL* locus. The results indicate that the *MLL* BCR is characterized by a specific chromatin structure that may be relevant to DNA cleavage and/or DNA repair.

Materials and Methods

Cells and Chromatin Preparation. Human T-cell leukemia Jurkat cells were cultured in RPMI 1640 containing 10% fetal bovine serum. Normal human CD34$^+$ cells were enriched from mobilized peripheral blood cells obtained from consenting healthy donors receiving recombinant human granulocyte colony-stimulating factor for stem cell mobilization purposes. CD34$^+$ cells were enriched according to a magnetic cell-sorting methodology (Miltenyi Biotec, Bergisch Gladbach, Germany). Briefly, nucleated cells were labeled with an anti-CD34 monoclonal antibody (QBEND/10) coupled to superparamagnetic microbeads. Labeled cells were then separated by a high gradient magnetic separation column placed in a strong magnetic field using the autoMACS instrument (Miltenyi Biotec). The separation method consistently yields highly purified cell samples containing ≥93% CD34$^+$ cells. Purified progenitor blood cells were not expanded *in vitro* and were used within 3 h of purification. During this time, CD34$^+$ cells were maintained in Iscove's modified Dulbecco's medium (Invitrogen, Milan, Italy) with 10% FCS and 4 mM glutamine and without human growth factors at 37°C in 5% CO_2.

Received 4/24/03; revised 1/9/04; accepted 2/17/04.

Grant support: This work was supported by the Associazione Italiana per la Ricerca sul Cancro, Milan; the Ministero dell' Istruzione, dell' Università e della Ricerca, under the PRIN E.F. 2001 program, Rome; and the Bologna University. C. Carlo-Stella is supported by Michelangelo Foundation for Advances in Cancer Research and Treatment (Milan, Italy). A. Khobta was supported by a Research Training Fellowship from the International Agency for Research on Cancer (IARC/R2913) and is on leave from the R. E. Kavetsky Institute of Experimental Pathology, Oncology and Radiobiology, National Academy of Sciences of Ukraine, Kyiv, Ukraine.

The costs of publication of this article were defrayed in part by the payment of page charges. This article must therefore be hereby marked *advertisement* in accordance with 18 U.S.C. Section 1734 solely to indicate this fact.

Requests for reprints: Giovanni Capranico, Department of Biochemistry, University of Bologna, via Irnerio 48, 40126 Bologna, Italy. Phone: 39-051-2094282; Fax: 39-051-2094283; E-mail: giovanni.capranico@unibo.it.

[3] J. L. Huret, 11q23 rearrangements in leukaemia. Atlas of Genetics and Cytogenetics in Oncology and Haematology. Updated August 2003. http://www.infobiogen.fr/services/chromcancer/Anomalies/11q23ID1030.html.

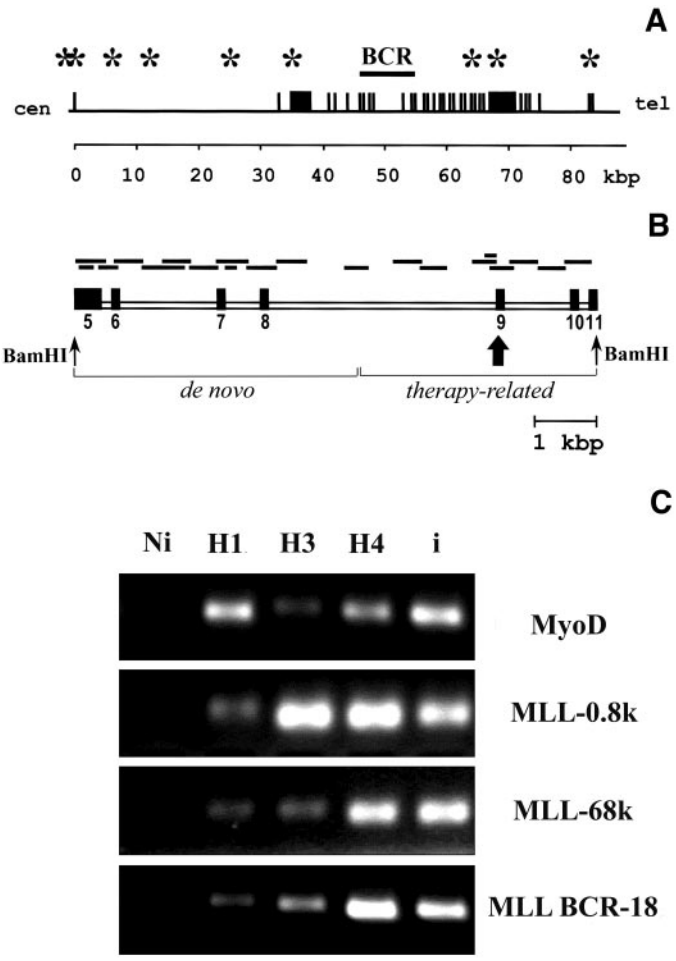

Fig. 1. *A*, diagram of the *MLL* gene. Exons are indicated by *boxes* starting from exon 1 on the *left*. Labels are as follows: cen, centromere; tel, telomere. Positions of PCR targets are marked with *asterisks* and further referred according to their distance in kb from the start of exon 1. The *MLL* BCR is shown with a *horizontal bar*. *B*, diagram of the *MLL* BCR. Exons are indicated with *boxes and numbers* (5). PCR products are indicated by *horizontal bars*. A DNase I-sensitive site near exon 9 is shown by a *bold arrow* (21). *Brackets*, "*de novo*" and "*therapy-related*," indicate the centromeric and telomeric BCR portions where translocation sites have preferentially been found in *de novo* and therapy-related leukemias, respectively (1, 3, 24). *C*, distinct histone patterns in Jurkat chromatin. Agarose gels of PCR products using X-ChIP DNA templates. PCR reactions were stopped during the exponential phase to keep band intensities proportional to DNA fragment recovery. *Lanes* are as follows: Ni, nonimmune IgG; H1, H3, and H4, antibodies to histones H1, acetylated H3, and acetylated H4, respectively; and i, 3% input DNA. Specificity of primers is indicated on the *right*: MyoD, exon 1 of *MyoD* gene; MLL-0.8K, a region centered 0.8 kbp downstream from the start of *MLL* gene exon 1; MLL-68K, e region 68 kbp distant from *MLL* exon 1 start; and MLL BCR-18, the region of BCR between 7001–7473 bp from the centromeric *BamH*1 site. *BCR*, breakpoint cluster region.

Normal human $CD34^+$ cells or Jurkat cells ($4–5 \times 10^5$ cells/ml) were either fixed directly with 1% formaldehyde for 15 min or treated with 5 mM Na-butyrate for 16 h before formaldehyde cross-linking. Jurkat cells in G_2-M phase were separated from growing cultures by using an Epics Elite ESP Flow cytometer (Beckman Coulter, Hialah, FL). Before sorting, cells were fixed with 1% formaldehyde for 1 h, washed twice with PBS, and stained with 50 μg/ml propidium iodide and 10 μg/ml RNase A. Sorted samples contained >90% of G_2-M phase cells.

To prepare chromatin, fixed cells were washed twice with ice-cold phosphate buffer followed by TEE (10 mM Tris-HCl, pH 8.0, 10 mM EDTA, 0.5 mM EGTA) containing 0.25% Triton X-100, TEE with 0.2 M NaCl, and resuspended in TEE. Protease inhibitors were added before use. Chromatin was then sheared by sonication with a Branson 250 sonifier (Branson Ultrasonic Corp., Danbury, CT) to an average DNA fragment size of 300–400 bp.

X-ChIP Procedure. A standard X-ChIP procedure was used (20). Briefly, immunoprecipitations were performed at 4°C in radioimmunoprecipitation assay buffer [50 mM Tris-HCl (pH 8.0), 1 mM EDTA, 0.5 mM EGTA, 150 mM NaCl, 1% Triton X-100, 0.1% Na-deoxycholate, 0.1% SDS]. Amounts of chromatin, equivalent to 0.5–0.8 $A_{260\ nm}$ were taken for each immunoprecipitation. Samples were precleared with 10 μg of preimmune rabbit IgG for 1 h followed by the addition of 40 μl of 50% suspension of 1:1 mix of Protein A- and Protein G-Sepharose beads for 1 h. One eleventh of the supernatants were saved as "10% input." Supernatants were incubated overnight with 10 μg of specific antibody or preimmune rabbit IgG. Anti-Ac-H3 and anti-Ac-H4 antibodies were purchased from Upstate (Lake Placid, NY). Anti-H1 antibody was from Santa Cruz Biotechnology (Santa Cruz, CA) and nonimmune rabbit IgG was from Cedarlane (Hornby, Canada). Immunocomplexes were recovered by addition of Protein A-/Protein G-Sepharose beads blocked with DNase-free BSA and salmon testes DNA. Then, immunopelletes were washed four times with radioimmunoprecipitation assay buffer; once with radioimmunoprecipitation assay buffer containing 0.5 M NaCl; once with 10 mM Tris-HCl (pH 8.0), 1 mM EDTA, 0.25 M LiCl, 0.5% Na-deoxycholate, and 0.5% NP40; twice with TE [10 mM Tris-HCl, 1 mM EDTA (pH 8.0)]; and finally resuspended in TE. To reverse cross-links, samples were adjusted to 0.5% SDS and incubated overnight at 65°C. After proteinase K treatments and phenol extractions, DNAs were ethanol-precipitated in the presence of 20 μg of glycogen (Roche Diagnostics, Manheim) and dissolved in TE. Recovered DNA was quantified by real-time PCR.

Quantitative Real-Time PCR. Real-time PCR was performed by using the LightCycler and the FastStart DNA Master SYBR Green I kit (Roche Diagnostics, Mannheim). Quantification and melting curve analyses were performed using the Roche LightCycler software by the crossing point method as indicated by the supplier. PCR reactions contained 1× FastStart DNA SYBR Green I Master Mix, 3 mM $MgCl_2$ and 350 nM each of primers. Specificity of PCR products was routinely controlled by melting curve analysis and agarose gel electrophoresis. At least four dilutions of input DNA were run to generate the standard curve, DNA recovery was thus measured as input DNA fraction.

Results

The BCR Chromatin of the *MLL* Gene Is Asymmetric by Histone H1 Content. We have mapped histone components of chromatin at the *MLL* locus in exponentially growing human Jurkat cells with X-ChIP method, and DNA fragment recovery was measured with real-time PCR as compared with input DNA. Twenty primer pairs covering the whole length of *MLL* BCR were designed, and nine primer pairs were chosen elsewhere across the *MLL* gene (Fig. 1, *A-B*). The *MLL* gene was studied in comparison to other loci: exon 1 of the *MyoD* gene (MyoD), chromosome 2-α-satellite DNA repeat (α-Sat-II), and a fragment located at nearly 46 kbp upstream to the *MLL* exon 1 that was predicted as a matrix-associated region (MAR) by computational analyses using MAR-Wiz tool.[4] The *MLL* gene was expressed in Jurkat cells, whereas the transcript of the *MyoD* gene was undetectable under the same conditions (data not shown).

First, histone H1 richness was measured along the *MLL* gene and the whole BCR (Fig. 2, *A* and *B*). In this report, DNA recovery data have been normalized relative to the recovery of the fragment spanning a BCR stretch from 7001 to 7473 bp (intron 9) from the centromeric *BamH*1 site (shown with an *open symbol* in all figures and indicated with *MLL* BCR-18 in Fig. 1*C*). Chromatin at the *MLL* gene promoter and in the region up to 12 kbp downstream from the ATG translation start was relatively poor in histone H1 since relative fragment recoveries were between 0.5 and 0.9 (Fig. 2*A*). From 25 kbp up to the end of the gene, histone H1 increased and remained relatively constant at 1.4–2.0 of relative recovery. Interestingly, chromatin at the *MLL* BCR was characterized by a generally higher content of histone H1, particularly at its centromeric portion where H1 peaked at around 1500 bp from the centromeric *BamH*1 site, corresponding to intron 6 (Fig. 2*B*). DNA recovery in that BCR portion was at levels (2–3 of relative recovery) very similar to those of α-Sat-II and MyoD

[4] http://www.futuresoft.org/MAR-Wiz/.

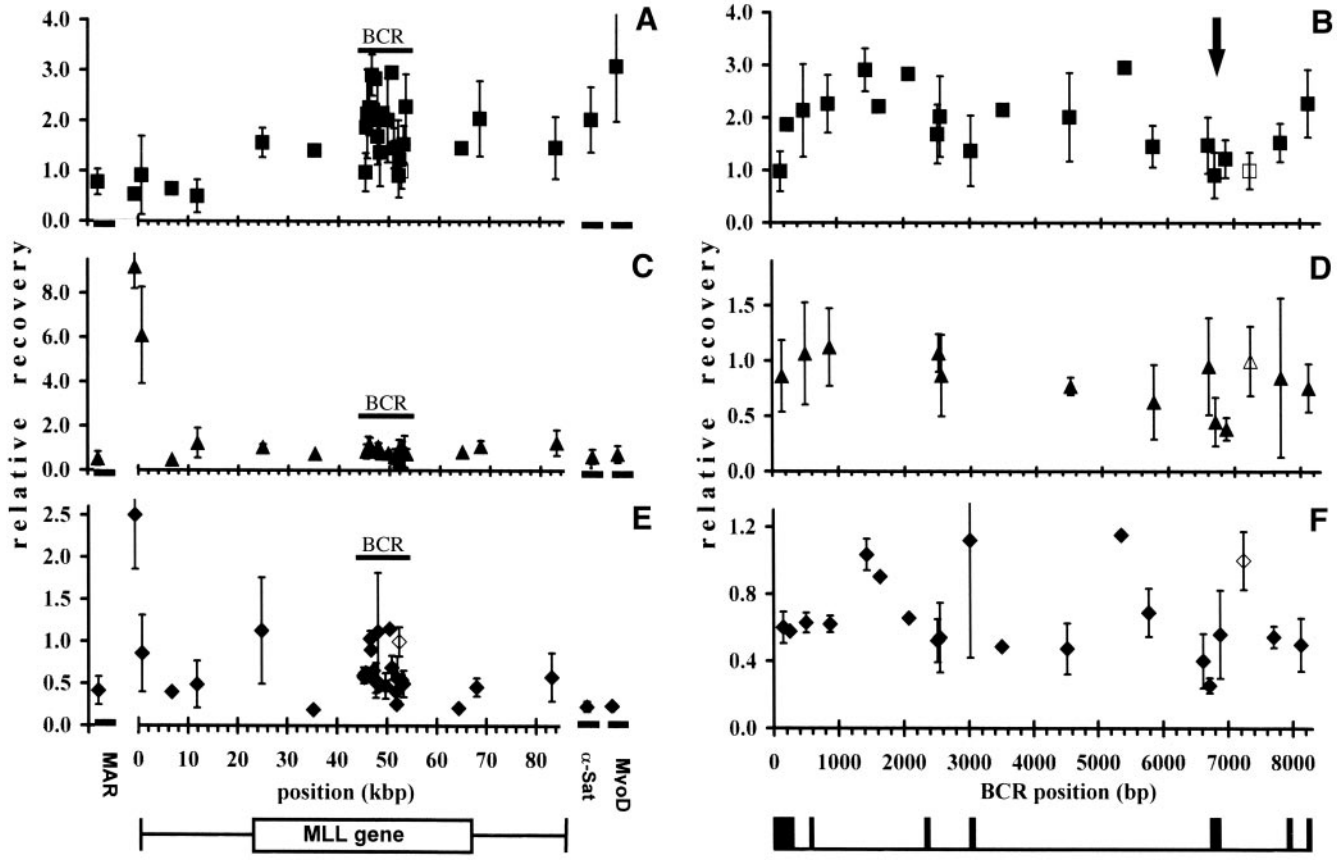

Fig. 2. Distribution of histone H1 (*A-B*) and of acetylated histones H3 (*C-D*) and H4 (*E-F*) across the *MLL* gene. The whole *MLL* gene (*A, C, E*) and the *MLL* BCR (*B, D, F*) are shown. Positions of exons 5–11 in the *MLL* BCR are indicated with *boxes*. A DNase I-sensitive site localizes immediately 5′ to exon 9 in the *MLL* BCR (21) and is indicated by an *arrow* in *B*. Values are means ± SE of up to 12 determinations. Recoveries of DNA fragments were quantified by real-time PCR as percentages of input and normalized relative to the same fragment (indicated with *open symbols*). *BCR*, breakpoint cluster region.

(Fig. 2, *A* and *B*), which likely have a repressed chromatin structure in Jurkat cells. At the same time, chromatin at 1100–1600 bp from the telomeric *BamH*1 site had a low H1 content (0.9–1.2 of relative recovery, Fig. 2*B*). This region extends over a MAR and a DNase I-sensitive site mapped at about 1.5 kbp from the telomeric end of BCR (6). Similarly, a predicted MAR fragment beyond the *MLL*-coding sequence start was poor in histone H1 (Fig. 2*A*).

Thus, the chromatin at the *MLL* BCR was heterogeneous in H1 contents, with a centromeric portion that had levels of histone H1 identical to the repressed chromatin of the MyoD gene promoter and α-Sat-II DNA and with relatively low H1 content at its telomeric part.

Acetylation of Histone H4 at Specific Sites of the *MLL* BCR. Next, we determined the extents of acetylation of H4 and H3 histones at the BCR and across the *MLL* gene (Fig. 2) by using antibodies that recognized acetylated Lys-9 and -14 of H3 and acetylated Lys-5, -8, -12, and -16 of H4. The highest observed acetylation of both histones was detected in correspondence to the promoter of *MLL* gene (Figs. 1*C* and 2, *C* and *E*). In contrast, it was low in MyoD fragment, without notable difference from α-satellite DNA. In case of acetyl-histone H3, *MLL* promoter and exon 1 fragments demonstrated relative recoveries of 9.2 and 6.1, respectively (Fig. 2*C*), that were at least one order of magnitude higher than all other fragments investigated. Within the *MLL* BCR, DNA fragment recoveries were rather similar, varying between 0.55 and 1.2 (Fig. 2*D*). Only a region centered at 6750 from the centromeric *BamH*1 site showed a lower level (0.35) of H3 acetylation that corresponded to a similarly low level of H4 acetylation (see below).

With the exception of three fragments, acetylation of histone H4 was higher across the *MLL* gene than at α-Sat-II and MyoD fragments (Fig. 1*C* and 2*E*) that were found in immunoprecipitates at about 0.2 of relative recovery, corresponding to a minimum of H4 acetylation. Similarly to H3, histone H4 was strongly acetylated at the *MLL* promoter region (about 2.5 of relative recovery), and the acetylation spread out partially on exon 1 (Fig. 2*E*). Excluding the promoter and adjacent region where acetylation might be linked to gene expression, a majority of fragments in the *MLL* (18 of 27) and the predicted MAR showed some H4 acetylation with relative recoveries in range 0.4–0.7 (Fig. 2, *E-F*). However, six fragments were recovered at higher levels (0.9–1.2), identifying four islands of increased H4 acetylation in the *MLL* BCR (Fig. 2, *E-F*) and one more spot in intron 1 (Fig. 2*E*). The four islands of H4 acetylation in the BCR were located near exon 8 and within introns 6, 8, and 9 (Fig. 2*F*). The latter two introns are adjacent to a site of low content of histone H1 (see Fig. 2*B*).

Hence, the *MLL* BCR chromatin was characterized by a uniformly low histone H3 acetylation, whereas histone H4 acetylation was more heterogeneous across the *MLL* BCR with defined islands of increased acetylation.

A Histone Deacetylase (HDAC) at Specific Sites of the *MLL* BCR. To establish whether the acetylation level of histones H3 and H4 is regulated by HDACs in *MLL* BCR, we studied the effect of sodium butyrate on histone modifications. Sodium butyrate is known to inhibit HDACs that act both on histones H3 and H4 (14). Jurkat cells were treated with 5 mM sodium butyrate for 16 h. Under this mode of treatment, no toxic effect of sodium butyrate was observed. Sodium butyrate treatments changed slightly the distribution of cell populations through the cell cycle increasing the amount of cells in G_2-M phase (34% of G_2-M phase cells *versus* 23% in control). Scanning X-ChIP was performed in parallel using the same amount of

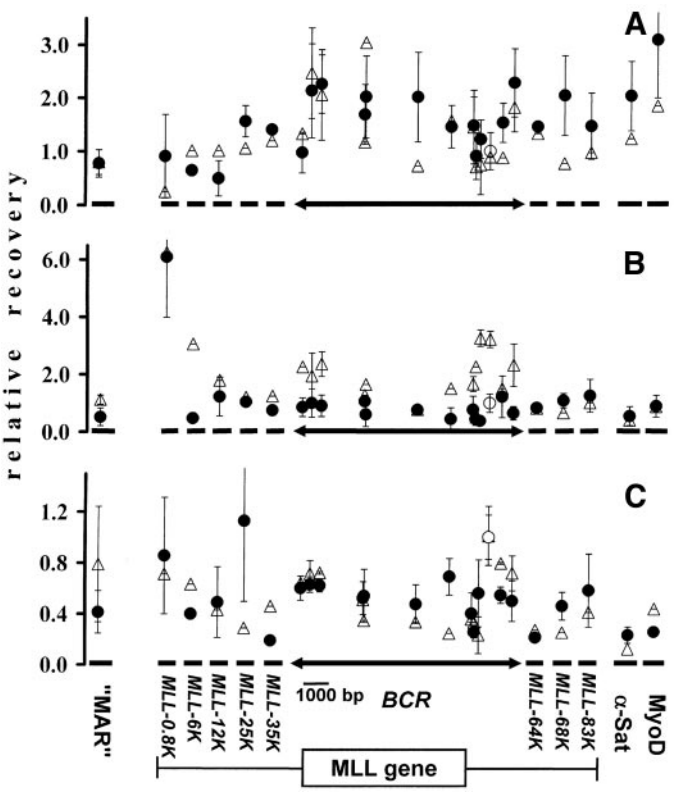

Fig. 3. Effect of butyrate on histone components in the *MLL* gene. Recoveries of DNA fragments with antibodies to histone H1, acetylated histones H3 and H4 (*A-C*, respectively), were quantified by real-time PCR as percentages of input and normalized as in Fig. 2. Means ± SE are shown for each DNA fragment. ●, control; △, 5 mM Na-butyrate added for 16 h. An *open circle* indicates the fragment used to define a unit of relative recovery. Only *MLL* BCR is represented in scale. PCR products are indicated below the *X* axis. *BCR*, breakpoint cluster region; *MAR*, matrix-associated region; MyoD, exon 1 of the *MyoD* gene; α-Sat, chromosome α-satellite.

cross-linked chromatin simultaneously isolated from control and butyrate-treated cells. Distribution of histone H1 underwent no significant changes after butyrate treatments, whereas acetylation of histone H3 was increased in a site-specific manner (Fig. 3, *A* and *B*). Some increase was observed in a group of neighboring fragments in the telomeric half of *MLL* BCR (maximal increase in relative recovery 3.3 against 0.4 in control) and near the centromeric end of the *MLL* BCR with relative recovery of 2–2.3, whereas it was 0.9–1 in control cells (Fig. 3*B*). In addition, histone H3 acetylation was increased by butyrate treatment at the fragment located 6 kbp downstream to the start of *MLL* coding sequence (relative recovery 3.1 against 0.5 in control cells). Surprisingly, no significant increase in histone H4 acetylation was detected in butyrate-treated cells as compared with control cells (Fig. 3*C*). These results thus suggest that an acetylase/deacetylase activity preferentially targeting histone H3 is likely present at the *MLL* BCR and localized at two spots of the telomeric and centromeric ends.

Histone Components at the *MLL* Gene BCR in G_2-M Phase Cells. We then performed X-ChIP by using chromatin of cells in G_2-M phase *versus* exponentially growing cells to establish whether histone components of chromatin change in dependence of cell-cycle phase and also whether sodium butyrate effects were a consequence of the observed shift of the cell population *versus* G_2-M phase. G_2-M phase cells were purified by cell sorting after formaldehyde cross-linking, and immunoprecipitations of chromatin from nonsorted and G_2-M phase cells were performed in parallel (Fig. 4, *A-C*). Increased histone H1 content was observed in the majority of tested regions in G_2-M phase cells with respect to nonsorted cells (Fig. 4*A*). Interestingly, regions that were poor in H1 in exponentially growing cells (Fig. 2, *A-B*) conserved a low H1 content in G_2-M phase as well. The *MLL* promoter and two adjacent fragments at the telomeric part of *MLL* BCR maintained a relative recovery of 1 as compared with 2.3–5 of the other fragments including MAR and α-Sat-II DNA (Fig. 4). Histone H3 and H4 acetylation patterns showed no significant changes in G_2-M phase cells with respect to nonsorted cells, although *MLL* promoter regions had slightly higher levels of both histone H3 and H4 acetylation in G_2-M phase than in exponentially growing cells (Fig. 4, *B* and *C*). Because cells in G_2-M phase did not show an increase of H3 acetylation within the BCR, the results thus suggested that butyrate effects were not mediated by perturbations of the cell distribution in cell-cycle phases.

Histone Components at the *MLL* Gene BCR in Normal Human $CD34^+$ Cells. Next, we determined the levels of H3 and H4 acetylation and H1 contents at the *MLL* BCR in human $CD34^+$ progenitor cells before and after treatments with butyrate for 16 h (Fig. 5). In agreement with results in Jurkat cells, histone H1 was distributed asymmetrically across the BCR with higher contents at the centromeric end (relative recoveries ranged from 2.0 to 2.7). Histone H1 showed a minimum of 0.5 at the 3′terminus of intron 8 (see MLL BCR-16 fragment in Fig. 5) in which a DNase I-sensitive site has been mapped previously (6, 21). The linker histone was also found at low levels (0.7–1) at the exon 1 (MLL-0.8K fragment) and two other BCR telomeric fragments (Fig. 5*A*), and its level was highest (5.0) at the α-Sat-II DNA. Differently from Jurkat cells, butyrate induced a marked increase in H1 levels, especially at exon 1 and the BCR telomeric end. Strikingly, histone H1 remained at low levels (1.0) at the region known to be a DNase I-sensitive site and was unchanged at the α-Sat-II DNA (Fig. 5, *A* and *D*).

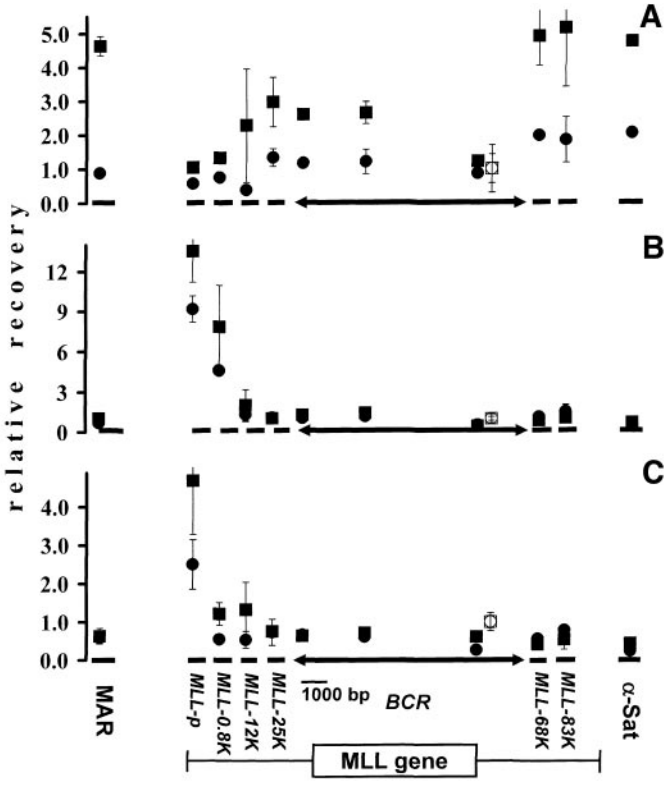

Fig. 4. Chromatin components at the *MLL* gene in the G_2-M phase. Chromatin preparations from nonsorted (●) or G_2-M phase (■) cells were immunoprecipitated in parallel. Recoveries of DNA fragments with antibodies specific to histone H1 and acetylated histones H3 and H4 (*A-C*, respectively) were measured by real-time PCR and normalized with the fragment indicated with *open symbols*. Values are means ± SE of two determinations. The *MLL* BCR is diagrammed in scale. PCR products are indicated below the *X* axis. MLL-p is a region at approximately 700 bp 5′ from the start of exon 1. *BCR*, breakpoint cluster region; *MAR*, matrix-associated region; α-Sat, chromosome α-satellite.

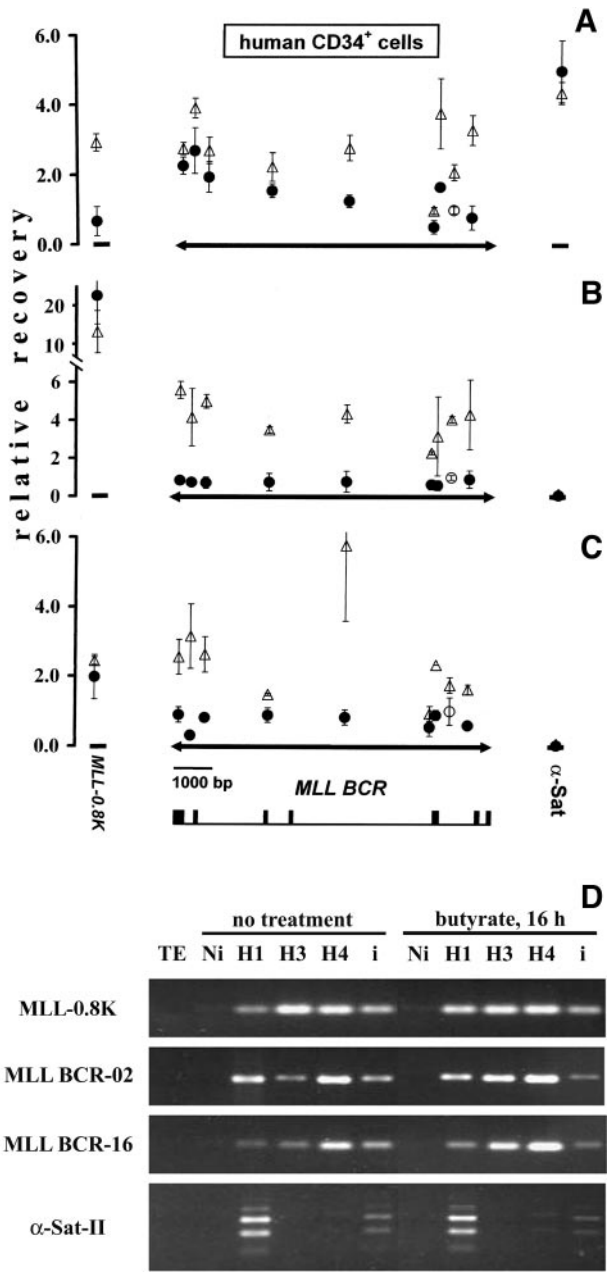

Fig. 5. Histone components at the *MLL* BCR in human hematopoietic CD34$^+$ cells and the effect of butyrate. *A-C*, fragment recoveries normalized as in Fig. 2. X-ChIP with antibodies to histone H1 (*A*) and acetylated histones H3 (*B*) and H4 (*C*). Average of two or three experimental values ±SE is shown for each DNA fragment. ●, control; △, 5 mM Na-butyrate added for 16 h. An *open circle* indicates the fragment used to define a unit of relative recovery. *MLL* BCR is represented in scale shown by a 1000 bp *horizontal bar*. Exons 5–11 in the *MLL* BCR are indicated with *boxes*. *D*, histone patterns in chromatin of human CD34$^+$ cells. *Lanes* are as follows: TE, no template; Ni, mock immunoprecipitation; H1, H3, and H4, immunoprecipitations with antibodies specific to histones H1, acetylated H3, and acetylated H4, respectively; and i, 1% input DNA. Purified DNAs were resuspended in TE, and the same amounts were used in PCR reactions. Genomic fragments are as follows: MLL-0.8K, a fragment 0.8 kbp from exon 1; MLL BCR-02, a region of intron 5 between 287–707 bp from the centromeric *BamH*1 site; MLL BCR-16, a region between 6617–6814 bp from the centromeric *BamH*1 site, corresponding to a DNase I hypersensitive site (21); and α-Sat-II, chromosome 2 α-satellite DNA. *BCR*, breakpoint cluster region.

α-Sat-II DNA was at very low levels in immuno-pellets of acetylated H3 and H4, 0.06 and 0.03, respectively (Fig. 5). In the studied BCR, histone H3 was slightly and uniformly acetylated (0.6–0.9 to be compared with 24.2 at *MLL* exon 1) and acetylation of histone H4 varied from 0.5 to 1.0 (2.0 in exon 1; Fig. 5, *B-D*). Butyrate treatments resulted in increased H3 and H4 acetylation particularly at the two ends of BCR but not at exon 1 (Fig. 5, *B* and *C*). Interestingly, acetylation increases of H3 and H4 were minimal at some BCR fragments including the DNase I-sensitive site.

Thus, in human CD34$^+$ progenitor blood cells, we have identified specific distinct histone modification patterns corresponding to centromeric and telomeric portions of the *MLL* gene BCR (Fig. 5*D*) that were in agreement with the findings in Jurkat cells. The MLL BCR-02 fragment was characteristic of the centromeric end with higher levels of histone H1, low and high acetylation of histones H3 and H4, respectively. Butyrate induced increases in H3 and H4 acetylation and some increase of H1 (Fig. 5*D*). The telomeric MLL BCR-16 fragment had the lowest histone H1 content, low H3 acetylation, and some acetylation of H4. Again, butyrate induced increases of core histone acetylation, whereas H1 remained at a minimum (Fig. 5*D*). The patterns were different from those observed at the MLL-0.8K fragment and the satellite DNA. The former demonstrated H3 hyperacetylation, high H4 acetylation, and low H1 content (Fig. 5*D*), and butyrate had no effects on histone acetylation but induced a dramatic increase of histone H1. The latter showed no histone acetylation and the highest H1 level and was unaffected by butyrate (Fig. 5*D*). Butyrate effects were in part different between Jurkat and CD34$^+$ cells, because only acetylated H3 increased in the former, whereas both core histones were more acetylated in the latter.

Discussion

In the present study, we have focused on histone modification patterns across the *MLL* gene and the *MLL* BCR in human Jurkat cells as well as in normal human CD34$^+$ progenitor cells. No abnormalities of chromosomes 11 are reported in Jurkat cells (22), thus allowing us to map histone modifications in the entire locus. The results demonstrate that, in both Jurkat and CD34$^+$ progenitor cells, the *MLL* BCR is characterized by a specific histone pattern, as follows: low H3 acetylation; islands of high H4 acetylation; and an asymmetric distribution of histone H1 (high and low at the centromeric and telomeric ends, respectively). Interestingly, histone H1 is specifically maintained at low levels at the telomeric end during G_2-M phase and after butyrate treatments. Moreover, specific butyrate-sensitive histone acetylase/deacetylase activities are present at the BCR in Jurkat cells and normal CD34$^+$ progenitor cells. The findings are relevant to the understanding of early molecular events leading to DNA cleavage and eventually to the repair and chromosome translocations at the *MLL* locus. We must note that normal human CD34$^+$ cells were collected from healthy donors after granulocyte colony-stimulating factor stimulation. Because the collected samples (containing ≥93% CD34$^+$ cells) were immediately treated with butyrate or maintained in fresh medium for 16 h before formaldehyde fixation, it is thus possible that marrow stimulation with growth factors might have altered chromatin structures of CD34$^+$ cells relative to unstimulated marrow cells.

Current knowledge of histone modifications provides an important link between chromatin structures and functions. Generally, acetylation of nucleosomes is associated with active chromatin and corresponds to more open conformations (13–16). According to the histone code hypothesis, in many cases the relationship between the acetylation of core histones and chromatin structure is complex. Specific acetylation of single lysines of histone tails together with other modifications may be crucial for transcriptional regulation (18). The analysis of bulk histone acetylation over a chromosomal locus can be extremely useful for the identification of chromatin domain boundaries or tissue-specific features of local chromatin structures. Moreover, increased acetylation of core histones has been demonstrated to correlate with hypersensitivity to DNase I digestion in distinct genomic loci (17).

Our findings showed that acetylation of histones H3 and H4 and the presence of histone H1 varied independently along the *MLL* gene. Distinct patterns could be evidenced in different genomic fragments (Figs. 1*C* and 5*D*) such as high H1 content and low H3 and H4 acetylation at repressed chromatin (MyoD and α-Sat II) and low H1 content and very highly acetylated H3 and H4 at the promoter of the *MLL* gene. In the transcribed region of the *MLL* gene, excluding 10–20 kbp at the 5′ side, H1 content was at an intermediate level, and H3 and H4 acetylation was low. Interestingly, the BCR showed a pattern different from other regions of the gene, as follows: high and low H1 contents at the centromeric and telomeric ends, respectively; islands of high H4 acetylation; and low H3 acetylation. A DNase I-sensitive site has been mapped immediately 5′ to exon 9 of *MLL* BCR (6, 21) that corresponded in our study to a site of low H1 content and low H3 and H4 acetylation, flanked at the telomeric side by a fragment of high H4 acetylation in Jurkat as well as in blood progenitor cells. The region maintained a relatively low H1 content during G_2-M phase in contrast to other regions that showed significantly increased levels of histone H1 with respect to nonsorted cells (Fig. 4*A*). In addition, a HDAC activity with a H3 preference may be present at the same BCR site. Thus, the BCR chromatin may have a particular organization that seems to be asymmetric because of the observed H1 distribution and a telomeric portion that shows peculiar features. In contrast to expression regulatory elements of a globin gene locus (23), core histones are not hyperacetylated at the reported DNase I-hypersensitive site of the human BCR, thus suggesting that sensitivity to nucleases is rather affected by low H1 content. Conversely, high contents of histone H1 in intron 6, which contains four *Alu* elements, can indicate a heterochromatin-like conformation. As discussed above, low H1 content may indicate regions of enhanced accessibility and hence be more available to nucleases. This feature of BCR chromatin may thus be relevant to early cleavage events rather than to illegitimate repair and chromosomal translocations, which may likely involve complex mechanisms including chromatin remodeling and sequence deletions and/or duplications (1, 24). A differential distribution of chromosomal breakpoints has been found in *MLL* BCR (Fig. 1); *e.g.*, in *de novo* and therapy-related patients, translocations preferentially fall to a centromeric and a telomeric portion, respectively (6). On the basis of present findings, one region may have a more compact structure and the other an open chromatin structure, respectively, (Fig. 2*B*, 4*A*, and 5*A*) therefore suggesting that mechanisms of chromosomal translocations and DNA repair may be different in the two cases. Interestingly, losses or insertions of vast regions of DNA were observed in *de novo* leukemias, whereas more precise recombinations with deletions or insertions of very few nucleotides were found in therapy-related cases suggesting different processing of DNA breaks during repair (24). An intriguing possibility is that the cellular choice of a DNA repair pathway may be influenced by the local chromatin structure.

Surprisingly, the levels of histone H1 were not high at the predicted MAR nor across the experimentally confirmed MAR in the telomeric half of the *MLL* BCR. The results are somewhat in contrast with earlier reports of preferential H1 assembly on MAR templates (25), although we have found a marked increase of H1 binding to the predicted MAR in G_2-M phase Jurkat cells but not at the BCR telomeric MAR (Fig. 4). Moreover, other cellular proteins, such as chromosomal proteins containing AT-hook motifs (26, 27) can compete with histone H1 and with each other for binding to MARs; thus different proteins may bind to MAR DNAs in a regulated fashion during cell cycle and differentiation. Interestingly, MAR DNAs can be hypersensitive to DNase I digestion, and our results document that the telomeric MAR at the *MLL* BCR is relatively free of H1. The findings thus suggest that a telomeric portion (centered at exon 9) may be characterized by a low nucleosome density and/or an open chromatin conformation. This may make the site more accessible to top2 and apoptotic nucleases. On the other hand, the centromeric portion of BCR may be less accessible to DNA-cleaving enzymes, although this does not rule out the possibility that enzymes may be recruited specifically at the centromeric half of BCR by protein interactions. It has to be noted that intron 6 in the centromeric half of the BCR contains four *Alu* repeats. It has been reported that the most frequently occurring chromosomal breakpoints that result in *MLL* partial duplications involve the *Alu* sequences in introns 1 and 6 (28, 29). Because elevated levels of histone H1 were found both at intron 6 and within intron 1 (Fig. 2, *A* and *B*), we suggest that a more closed chromatin structure may help to prevent *Alu* repeats from recombining with other unrelated regions (30). However, this remains to be fully established. We have begun to elucidate the chromatin structure at *MLL* gene breakpoints, and a global genomic approach to the study of chromatin components may provide additional information on the relevance of histone patterns on the molecular events leading to cell transformation.

The cellular context may influence chromatin components as shown by some different effects of butyrate on histone modifications at BCR in Jurkat and progenitor blood cells. Acetylation of histone H3 increased after butyrate exposures in a portion of *MLL* intron 9 and, to a lesser extent, near the centromeric end of the BCR in Jurkat cells. It can be noted that, under our conditions, the consistent response to butyrate was generally low at the *MLL* locus in Jurkat cells; *e.g.*, H4 acetylation was not increased and that of H3 was also not increased at several tested regions (Fig. 3). Thus, given the general low response, the detected increased histone acetylation at the two ends of BCR may indicate that a HDAC particularly sensitive to butyrate is present at these regions in Jurkat cells. The response to butyrate was generally higher in blood progenitor cells; however, core histone acetylation very close to the *MLL* promoter was not increased by butyrate, and acetylation of H4 was increased less than H3 (Fig. 5). Therefore, we suggest that the two BCR ends are sites of a HDAC activity preferentially targeting H3 histone in Jurkat cells. Such a preference for H3 histone is attenuated in our collected human progenitor blood cells. Interestingly, human top2 isoforms were shown to interact with HDAC1 and 2 (31, 32); however, whether a top2-HDAC complex is present at the *MLL* BCR remains to be established. Histone deacetylase/acetylase activities can be critical for chromatin organization and therefore may influence the occurrence of chromosomal breakpoints leading to rearrangements of the human *MLL* gene. However, the cell context must be taken into consideration in future studies to identify the mechanisms of chromosomal translocations relevant to human leukemias.

Acknowledgments

We thank D. Matteuzzi and P. Brigidi for the use of an ultrasonic processor, G. Farruggia for cell flow cytometry and sorting, and V. Orlando for advice on X-ChIP. We also thank the C.I.R.B. (Centro Interdipartimentale per le Ricerche Biotecnologiche), University of Bologna, for making critical facilities available.

References

1. Rowley JD. The critical role of chromosome translocations in human leukemias. Annu Rev Genet 1998;32:495–519.
2. Andersen MK, Christiansen DH, Jensen BA, Ernst P, Hauge G, Pedersen-Bjergaard J. Therapy-related acute lymphoblastic leukaemia with MLL rearrangements following DNA topoisomerase II inhibitors, an increasing problem: report on two new cases and review of the literature since 1992. Br J Haematol 2001;114:539–43.
3. Felix CA. Leukemias related to treatment with DNA topoisomerase II inhibitors. Med Pediatr Oncol 2001;36:525–35.
4. Strick R, Strissel PL, Borgers S, Smith SL, Rowley JD. Dietary bioflavonoids induce cleavage in the MLL gene and may contribute to infant leukemia. Proc Natl Acad Sci USA 2000;97:4790–5.

5. Rasio D, Schichman SA, Negrini M, Canaani E, Croce CM. Complete exon structure of the ALL1 gene. Cancer Res 1996;56:1766–9.
6. Strissel Broeker PL, Super HG, Thirman MJ, et al. Distribution of 11q23 breakpoints within the MLL breakpoint cluster region in de novo acute leukemia and in treatment-related acute myeloid leukemia: correlation with scaffold attachment regions and topoisomerase II consensus binding sites. Blood 1996;87:1912–22.
7. Stanulla M, Wang J, Chervinsky DS, Thandla S, Aplan PD. DNA cleavage within the MLL breakpoint cluster region is a specific event which occurs as part of higher-order chromatin fragmentation during the initial stages of apoptosis. Mol Cell Biol 1997; 17:4070–9.
8. Betti CJ, Villalobos MJ, Diaz MO, Vaughan AT. Apoptotic triggers initiate translocations within the MLL gene involving the nonhomologous end joining repair system. Cancer Res 2001;61:4550–5.
9. Sim SP, Liu LF. Nucleolytic cleavage of the mixed lineage leukemia breakpoint cluster region during apoptosis. J Biol Chem 2001;276:31590–5.
10. Pommier Y, Orr A, Kohn KW, Riou JF. Differential effects of amsacrine and epipodophyllotoxins on topoisomerase II cleavage in the human c-myc protooncogene. Cancer Res 1992;52:3125–30.
11. Borgnetto ME, Zunino F, Tinelli S, Kas E, Capranico G. Drug-specific sites of topoisomerase II DNA cleavage in Drosophila chromatin: heterogeneous localization and reversibility. Cancer Res 1996;56:1855–62.
12. Binaschi M, Borgnetto ME, Capranico G. Loss of drug-stimulated topoisomerase II DNA breaks in living cells is different at two unrelated loci. Nucleic Acids Res 2000;28:3289–93.
13. Luger K, Richmond TJ. The histone tails of the nucleosome. Curr Opin Genet Dev 1998;8:140–6.
14. Kornberg RD, Lorch Y. Twenty-five years of the nucleosome, fundamental particle of the eukaryote chromosome. Cell 1999;98:285–94.
15. Jenuwein T, Allis CD. Translating the histone code. Science (Wash D C) 2001;293: 1074–80.
16. Kurdistani SK, Grunstein M. Histone acetylation and deacetylation in yeast. Nat Rev Mol Cell Biol 2003;4:276–84.
17. Hebbes TR, Clayton AL, Thorne AW, Crane-Robinson C. Core histone hyperacetylation co-maps with generalized DNase I sensitivity in the chicken β-globin chromosomal domain. EMBO J 1994;13:1823–30.
18. Agalioti T, Chen G, Thanos D. Deciphering the transcriptional histone acetylation code for a human gene. Cell 2002;111:381–92.
19. Ura K, Kurumizaka H, Dimitrov S, Almouzni G, Wolffe AP. Histone acetylation: influence on transcription, nucleosome mobility and positioning, and linker histone-dependent transcriptional repression. EMBO J 1997;16:2096–107.
20. Orlando V, Strutt H, Paro R. Analysis of chromatin structure by in vivo formaldehyde cross-linking. Methods 1997;11:205–14.
21. Strissel PL, Strick R, Rowley JD, Zeleznik-Le NJ. An in vivo topoisomerase II cleavage site and a DNase I hypersensitive site colocalize near exon 9 in the MLL breakpoint cluster region. Blood 1998;92:3793–803.
22. Gebhart E, Thoma K, Verdorfer I, Drexler HG, Efferth T. Genomic imbalances in T-cell acute lymphoblastic leukemia cell lines. Int J Oncol 2002;21:887–94.
23. Anguita E, Johnson CA, Wood WG, Turner BM, Higgs DR. Identification of a conserved erythroid specific domain of histone acetylation across the α-globin gene cluster. Proc Natl Acad Sci USA 2001;98:12114–9.
24. Raffini LJ, Slater DJ, Rappaport EF, et al. Panhandle and reverse-panhandle PCR enable cloning of der(11) and der(other) genomic breakpoint junctions of MLL translocations and identify complex translocation of MLL, AF-4, and CDK6. Proc Natl Acad Sci USA 2002;99:4568–73.
25. Izaurralde E, Kas E, Laemmli UK. Highly preferential nucleation of histone H1 assembly on scaffold-associated regions. J Mol Biol 1989;210:573–85.
26. Zhao K, Kas E, Gonzalez E, Laemmli UK. SAR-dependent mobilization of histone H1 by HMG-I/Y in vitro: HMG-I/Y is enriched in H1-depleted chromatin. EMBO J 1993;12:3237–47.
27. Aulner N, Monod C, Mandicourt G, et al. The AT-hook protein D1 is essential for Drosophila melanogaster development and is implicated in position-effect variegation. Mol Cell Biol 2002;22:1218–32.
28. Schichman SA, Caligiuri MA, Strout MP, et al. ALL-1 tandem duplication in acute myeloid leukemia with a normal karyotype involves homologous recombination between Alu elements. Cancer Res 1994;54:4277–80.
29. Strout MP, Marcucci G, Bloomfield CD, Caligiuri MA. The partial tandem duplication of ALL1 (MLL) is consistently generated by Alu-mediated homologous recombination in acute myeloid leukemia. Proc Natl Acad Sci USA 1998;95:2390–5.
30. Wolffe AP, Matzke MA. Epigenetics: regulation through repression. Science (Wash D C) 1999;286:481–6.
31. Tsai SC, Valkov N, Yang WM, Gump J, Sullivan D, Seto E. Histone deacetylase interacts directly with DNA topoisomerase II. Nat Genet 2000;26:349–53.
32. Johnson CA, Padget K, Austin CA, Turner BM. Deacetylase activity associates with topoisomerase II and is necessary for etoposide-induced apoptosis. J Biol Chem 2001;276:4539–42.